Supporting Information

In-Situ Detection of the Adsorbed Fe(II) Intermediate and the Mechanism of Magnetite Electrodeposition by Scanning Electrochemical Microscopy

Mohsin A Bhat,[#,†] Nikoloz Nioradze,[‡] Jiyeon Kim,[§] Shigeru Amemiya,[¶] and Allen J. Bard[*,#]

[#] *Center for Electrochemistry, Department of Chemistry, The University of Texas at Austin, Austin, Texas 78712, United States*

[†] *Department of Chemistry, University of Kashmir, Srinagar-190006, J&K, India*

[‡] *The R. Agladze Institute of Inorganic Chemistry and Electrochemistry, Ivane Javakhishvili Tbilisi State University, Tbilisi 0179, Georgia*

[§] *Department of Chemistry, The University of Rhode Island, Kingston, Rhode Island 02881, United States*

[¶] *Department of Chemistry, University of Pittsburgh, Pittsburgh, Pennsylvania 15260, United States*

[*] To whom correspondence should be addressed. E-mail: ajbard@cm.utexas.edu.

Tip Characterization. The inner and outer radii of Au tips were determined by optical microscopy and approach curve measurement at insulating TiO_2 substrates (Figure S-1). The theoretical curve was calculated using an analytical equation reported in ref. S-1.

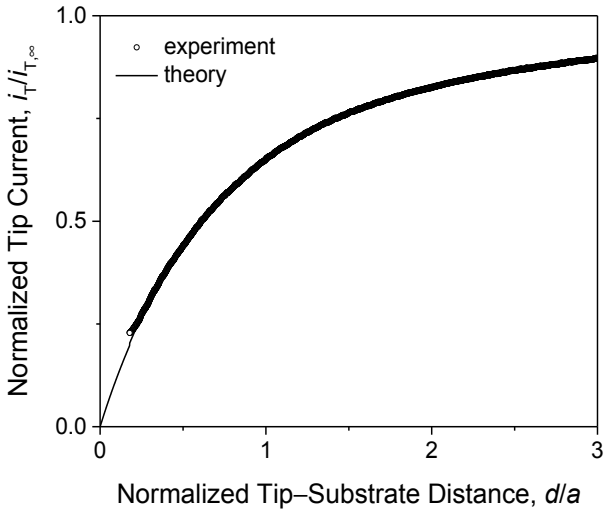

Figure S-1. Experimental (circles) and theoretical (solid line) SECM approach curves in the negative feedback mode as obtained with a 25 μm-diameter Au tip (RG = 3.0) over a TiO_2 substrate in a 0.1 M KNO_3 solution containing 1 mM ferrocenemethanol as a redox mediator. E_T = 0.33 V vs Ag/AgCl. Probe scan rate, 50 nm/s.

Optimization of Potential Sweep Rate. We investigated SECM-based CV of the Fe(III)–TEA/ Fe(II)–TEA couple at a wide range of potential sweep rate (1 mV/s–500 mV/s) in the feedback mode to find that the highest reverse peak was observed at 25 mV/s. When the potential sweep rate was faster than 25 mV/s, the reverse peak was broader and lower to eventually loose a peak shape at 500 mV/s (Figure S-2). A potential sweep rate of <25 mV/s yielded a lower peak-shaped response, which is quantitatively analyzed below (see Figure S-5).

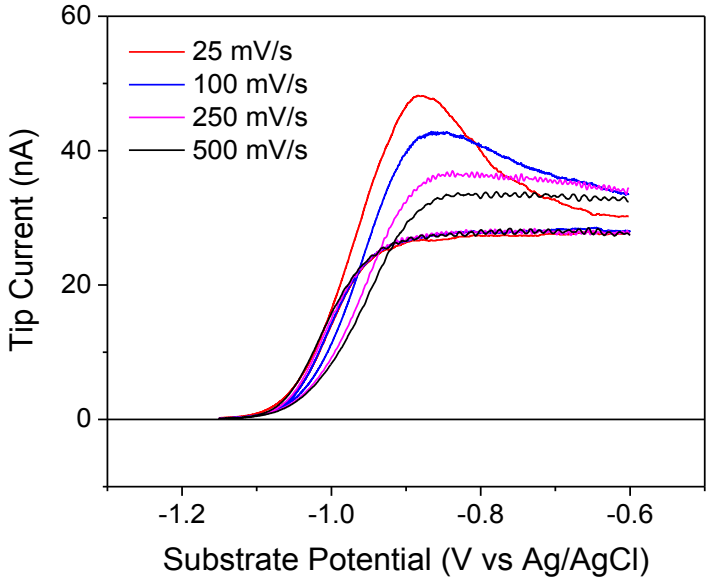

Figure S-2. Experimental SECM-based CVs at different potential sweep rates as obtained with a 25 µm-diameter Au tip (E_T = –1.15 V vs Ag/AgCl) at a 2 mm-diameter Au substrate in a 5 M NaOH solution containing 5 mM Fe(III)–TEA.

Model. Here we define a theoretical model to quantitatively describe SECM-based CVs for the electrodeposition and electrodissolution of magnetite in feedback and SG/TC modes. We consider an SECM configuration in the cylindrical coordinate (Figure S-3) to define the following diffusion problem.

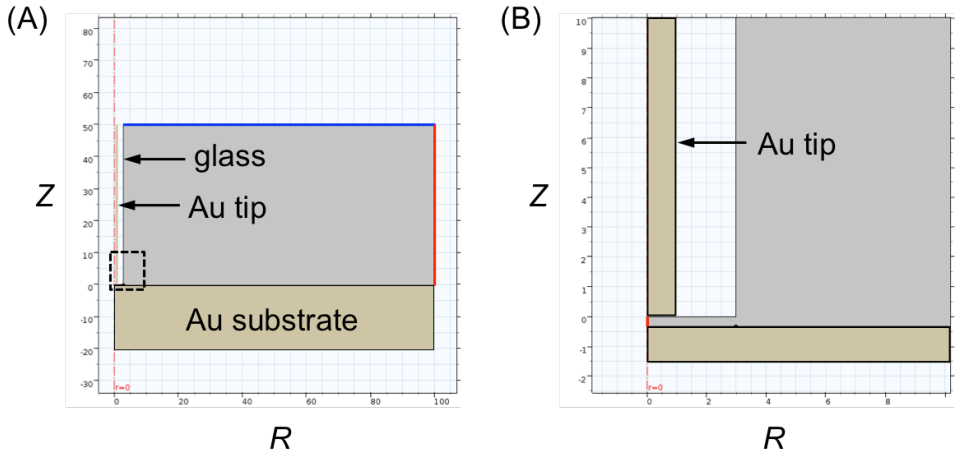

Figure S-3. (A) Scheme of the SECM configuration with a glass-insulated Au tip positioned at d/a = 0.33 from a macroscopic Au substrate. Part (B) represents the region of part (A) surrounded by the dashed box. Red boundaries show no normal flux. The blue boundary represents the bulk solution.

Specifically, we solved diffusion equations for species, i (= Fe(III)–TEA or Fe(II)–TEA as also represented by Fe(III) and Fe(II) in the following)

$$\frac{\partial c_{\mathrm{i}}}{\partial t} = D_{\mathrm{i}}\left[\frac{\partial^2 c_{\mathrm{i}}}{\partial r^2} + \frac{1}{r}\frac{\partial c_{\mathrm{i}}}{\partial r} + \frac{\partial^2 c_{\mathrm{i}}}{\partial z^2}\right] \qquad \text{(S-1)}$$

where D_{i} is the diffusion coefficient of species i. When the cycle of the substrate potential is initiated at t = 0, the tip potential is stepped to reduce Fe(III)–TEA in the feedback mode or oxidize Fe(II)–TEA in the SG/TC mode at diffusion-limited rates to yield the corresponding boundary conditions at the tip.[S-2] Boundary conditions at the Au substrate are given by considering the $EC_{ads}C_{mag}$ mechanism as follows,

whereas other boundary conditions are given in Figure S-1. The rate of the electron-transfer reaction (eq 1), v_{et}, is given by

$$v_{et} = k_{red} c_{Fe(III)} - k_{ox} c_{Fe(II)} \tag{S-2}$$

The adsorption rate of Fe(II)–TEA (eq 3), v_{ads}, is given by

$$v_{ads} = k_{ads} \left[c_{Fe(II)} \left(\Gamma^{0}_{Fe(II)} - \Gamma_{Fe(II)} \right) - \frac{\Gamma_{Fe(II)}}{\beta_{Fe(II)}} \right] \tag{S-3}$$

Finally, the formation of magnetite (eq 4) proceeds at the rate, v_m, as given by

$$v_m = k_{m,f} \left\{ \left[c_{Fe(III)} \right]^2 \Gamma_{Fe(II)} - \frac{\Gamma_{Fe_3O_4}}{K_m} \right\} \tag{S-4}$$

where $\Gamma_{Fe_3O_4}$ is the concentration of magnetite at the substrate surface. Overall, boundary conditions at the substrate surface are given by

$$D_{Fe(II)} \left[\frac{\partial c_{Fe(II)}}{\partial z} \right]_{z=-d} = v_{et} - v_{ads} \tag{S-5}$$

$$D_{Fe(III)} \left[\frac{\partial c_{Fe(III)}}{\partial z} \right]_{z=-d} = -v_{et} - 2v_m \tag{S-6}$$

$$\left[\frac{\partial \Gamma_{Fe(II)}}{\partial t} \right] = v_{ads} - v_m \tag{S-7}$$

$$\left[\frac{\partial \Gamma_{Fe_3O_4}}{\partial t} \right] = v_m \tag{S-8}$$

Dimensionless Parameters. The aforementioned model is defined by using the following dimensionless parameters and solved by using a commercial finite element simulation package,

Multiphysics 5.3 (COMSOL, Burlington, MA). Specifically, diffusion equations in dimensionless forms are defined from eq S-1 as

$$\frac{\partial C_{\mathrm{Fe(II)}}}{\partial \tau} = \gamma \left[\frac{\partial^2 C_{\mathrm{Fe(II)}}}{\partial R^2} + \frac{1}{R}\frac{\partial C_{\mathrm{Fe(II)}}}{\partial R} + \frac{\partial^2 C_{\mathrm{Fe(II)}}}{\partial Z^2} \right] \tag{S-9}$$

$$\frac{\partial C_{\mathrm{Fe(III)}}}{\partial \tau} = \left[\frac{\partial^2 C_{\mathrm{Fe(III)}}}{\partial R^2} + \frac{1}{R}\frac{\partial C_{\mathrm{Fe(III)}}}{\partial R} + \frac{\partial^2 C_{\mathrm{Fe(III)}}}{\partial Z^2} \right] \tag{S-10}$$

with

$$C_{\mathrm{i}} = \frac{c_{\mathrm{i}}}{c_0} \tag{S-11}$$

$$R = \frac{r}{a} \tag{S-12}$$

$$Z = \frac{z}{a} \tag{S-13}$$

$$\tau = \frac{D_{\mathrm{Fe(III)}} t}{a^2} \tag{S-14}$$

$$\gamma = \frac{D_{\mathrm{Fe(II)}}}{D_{\mathrm{Fe(III)}}} \tag{S-15}$$

In addition, the potential sweep rate, v, is converted to the dimensionless form, σ, as

$$\sigma = \frac{a^2 v F}{D_{\mathrm{Fe(III)}} RT} \tag{S-16}$$

Importantly, mass transport across the tip–substrate gap maintains a quasi-steady state when $\sigma < 1$.[S-2] Boundary conditions at the substrate surface (eqs S-5–S-8) are given by using dimensionless rates, V_{et}, V_{ads}, and V_{m} as

$$\gamma\left[\frac{\partial C_{\mathrm{Fe(II)}}}{\partial Z}\right]_{Z=-L} = V_{\mathrm{et}} - V_{\mathrm{ads}} \tag{S-17}$$

$$\left[\frac{\partial C_{\mathrm{Fe(III)}}}{\partial Z}\right]_{Z=-L} = -V_{\mathrm{et}} - 2V_{\mathrm{m}} \tag{S-18}$$

$$\left[\frac{\partial \theta_{\mathrm{Fe(II)}}}{\partial \tau}\right] = V_{\mathrm{ads}} - V_{\mathrm{m}} \tag{S-19}$$

$$\left[\frac{\partial \theta_{\mathrm{Fe_3O_4}}}{\partial \tau}\right] = V_{\mathrm{m}} \tag{S-20}$$

These equations include additional dimensionless parameters

$$L = \frac{d}{a} \tag{S-21}$$

$$\theta_{\mathrm{j}} = \frac{\Gamma_{\mathrm{j}}}{ac_0} \tag{S-22}$$

where j is represented by Fe(II) for the adsorbed Fe(II) intermediate or Fe_3O_4 for magnetite. Each dimensionless rate is given as follows. The dimensionless electron-transfer rate, V_{et}, is given by

$$V_{\mathrm{et}} = \lambda\left(1 - \frac{\theta_{\mathrm{Fe(II)}}}{\theta^0_{\mathrm{Fe(II)}}}\right)\left[\theta_{\mathrm{S}}^{-\alpha} C_{\mathrm{Fe(III)}} - \theta_{\mathrm{S}}^{(1-\alpha)} C_{\mathrm{Fe(II)}}\right] \tag{S-23}$$

with

$$\lambda = \frac{k^0 a}{D_{\mathrm{Fe(III)}}} \tag{S-24}$$

$$\theta^0_{\mathrm{Fe(II)}} = \frac{\Gamma^0_{\mathrm{Fe(II)}}}{ac_0} \tag{S-25}$$

$$\theta_{\mathrm{S}} = \exp\left[\frac{F(E_{\mathrm{S}} - E^{0'})}{RT}\right] \tag{S-26}$$

The adsorption rate is defined in the dimensionless form, V_{ads}, as

$$V_{\mathrm{ads}} = \kappa_{\mathrm{ads}}\left\{\theta_{\mathrm{d}}^{\beta} C_{\mathrm{Fe(II)}}\left[\theta^{0}_{\mathrm{Fe(II)}} - \theta_{\mathrm{Fe(II)}}\right] - \theta_{\mathrm{d}}^{(\beta-1)}\frac{\theta_{\mathrm{Fe(II)}}}{\Lambda_{\mathrm{Fe(II)}}}\right\} \tag{S-27}$$

with

$$\kappa_{\mathrm{ads}} = \frac{ka^2 c_0}{D_{\mathrm{Fe(III)}}} \tag{S-28}$$

$$\theta_{\mathrm{d}} = \exp\left(g'\frac{\theta_{\mathrm{Fe(II)}}}{\theta^{0}_{\mathrm{Fe(II)}}}\right) \tag{S-29}$$

$$\Lambda_{\mathrm{Fe(II)}} = c_0 \beta_{\mathrm{Fe(II)}} \tag{S-30}$$

Finally, the dimensionless rate of the deposition of magnetite, V_{m}, is given by

$$V_{\mathrm{m}} = \kappa_{\mathrm{m,f}}\left\{\left[C_{\mathrm{Fe(III)}}\right]^2 \theta_{\mathrm{Fe(II)}} - \frac{\theta_{\mathrm{Fe_3O_4}}}{\Lambda_{\mathrm{m}}}\right\} \tag{S-31}$$

with

$$\kappa_{\mathrm{m,f}} = \frac{k_{\mathrm{m,f}} a^2 c_0^2}{D_{\mathrm{Fe(III)}}} \tag{S-32}$$

$$\Lambda_{\mathrm{m}} = c_0^2 K_{\mathrm{m}} \tag{S-33}$$

Finite Element Analysis of SECM-Based CVs by the Method of Least Squares. We employed the method of least squares based on the Optimization module of COMSOL Multiphysics as a quantitative approach to demonstrate that only narrow ranges of reaction parameters give good fits for both feedback and SG/TC branches of SECM-based CV. First, we determined the best set of eight reaction parameters (Table S-1) that gave the lowest total residual sum of squares when both feedback and SG/TC branches of experimental SECM-based CVs were fitted with simulation (Figures S-4A and S-4B, respectively). Then, we determined sets of parameters that gave the lowest residual sum of squares to fit only feedback or SG/TC branch with simulation. These sets of parameters were found to define lower or upper limits of parameters that give good fits for both branches as explained in the following. When we evaluated only the feedback branch, a slightly better fit was obtained (see the blue arrow in Figures S-4C) in comparison with the fit of the same branch by the best set of parameters. The fit of the SG/TC branch, however, was significantly compromised (see the red arrow in Figure S-4D) to subsequently yield a larger total residual sum of squares. Thus, the parameters determined only from the best fit of the feedback branch (Table S-1) represent limits of parameters at one side beyond which the fit of the SG/TC branch was significantly compromised. Limits of parameters at the other side were set by the parameters (Table S-1) that gave the best fit only for the SG/TC branch (Figure S-4F), because these parameters significantly compromised the fit of the feedback branch (Figure S-4E) to yield a higher total residual sum of squares. More specifically, these parameters improved the fit of the SG/TC branch around the switching potential (see blue arrows in Figure S-4F), but compromised fits of both SG/TC and feedback branches around peak potentials (see red arrows in Figures S-4F and S-4E, respectively). Overall, five parameters ($\beta_{\mathrm{Fe(II)}}$, g', $\Gamma^{0}_{\mathrm{Fe(II)}}$, $k_{\mathrm{m,f}}$, and K_{m}) determined from the best fit of both feedback and SG/TC branches (e.g., $\beta_{\mathrm{Fe(II)}} = 1.4$ in Table S-1) were found within narrow ranges between parameters determined from the best fit of either feedback or SG/TC branch (e.g., $\beta_{\mathrm{Fe(II)}} = 1.6$

and 1.3, respectively), thereby defining narrow ranges of parameters that gave good fits for both branches. By contrast, the $E^{0'}$ and k values determined from the best fit of both branches set lower limits while upper limits were set by the $E^{0'}$ and k values determined from the best fit of the SG/TC branch. The resultant ranges of these parameters were still narrow. Finally, a unique k^0 value of 0.13 cm/s was obtained to represent a kinetic limit when an inhibitory effect of the adsorbed Fe(II) intermediate on the ET kinetics (eq 10) was significant during the reverse sweep in the SG/TC mode.

Table S-1. Reaction Parameters of Magnetite Electrodeposition Determined from Feedback and/or SG/TC Branch of SECM-Based CV by the Method of Least Squares.[a]

Fitted branch	Both[a]	Feedback[b,c]		SG/TC[c,d]	
k^0 (cm/s)	0.13	0.13	(0%)	0.13	(0%)
$E^{0'}$ (V vs. Ag/AgCl)	–1.047	–1.045	(+0.2%)	–1.041	(+0.6%)
k (10^5 cm^3/s/mol)	1.9	2.1	(+11%)	2.4	(+26%)
$\beta_{Fe(II)}$ (10^5 cm^3/mol)	1.4	1.6	(+14%)	1.3	(–7%)
g'	3.2	3.1	(–3%)	3.5	(+9%)
$\Gamma^0_{Fe(II)}$ (10^{-9} mol/cm^2)	5.4	5.2	(–4%)	5.6	(+4%)
$k_{m,f}$ (10^{10} cm^6/s/mol^2)	1.4	1.4	(0%)	0.9	(–35%)
K_m (10^{10} cm^6/mol^2)	2.3	2.1	(–9%)	2.4	(+4%)

[a] Figures S-4A and S-4B. [b] Figures S-4C and S-4D. [c] Percentages in brackets indicate relative deviations from the values determined from both branches. [d] Figures S-4E and S-4F.

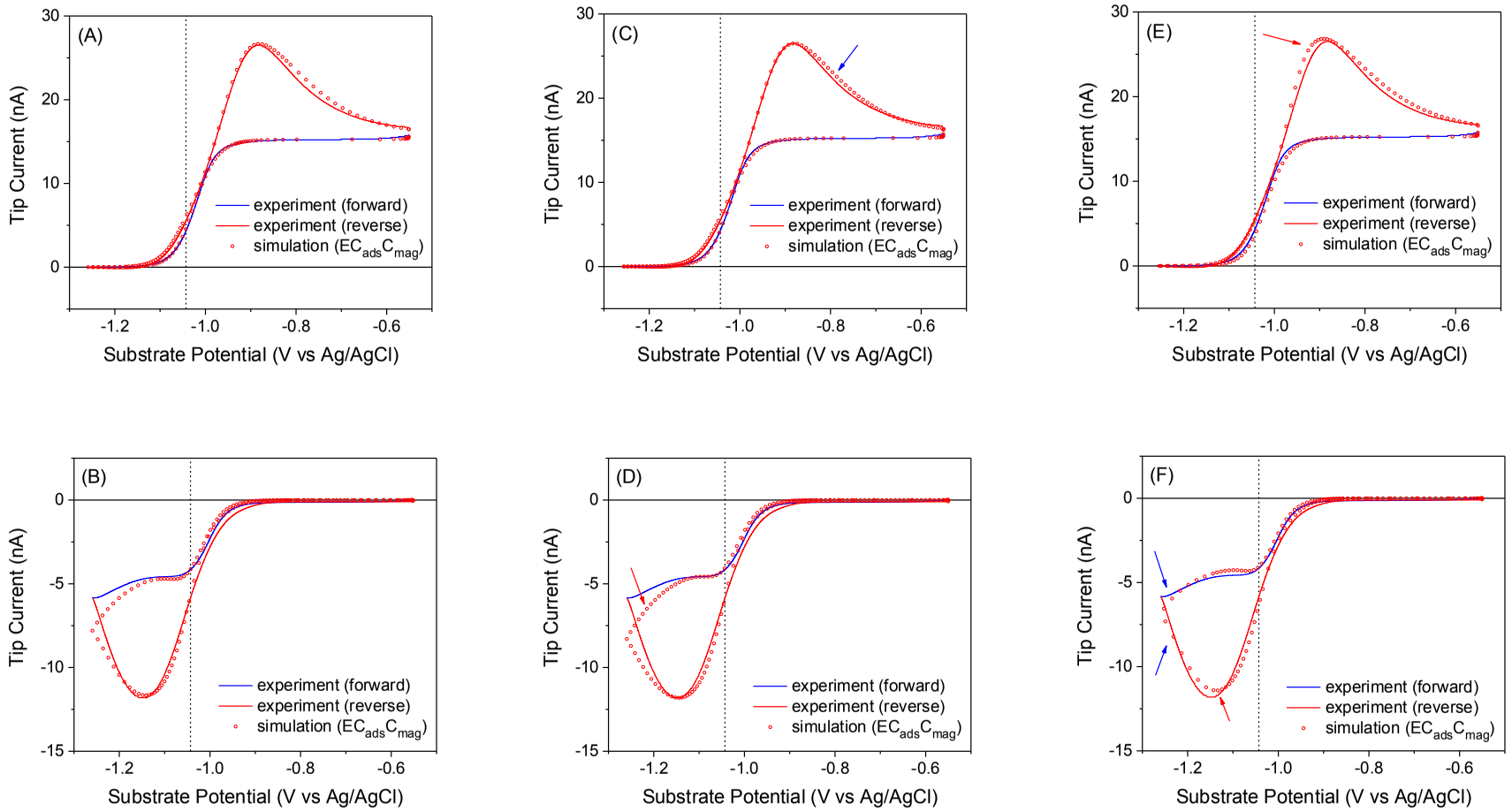

Figure S-4. Experimental and simulated SECM CVs in (A), (C), and (E) feedback and (B), (D), and (F) SG/TC mode. Simulated SECM CVs are based on the best fit to (A) and (B) both branches, (C) and (D) the feedback branch, and (E) and (F) SG/TC branch by the least squares method of COMSOL Multiphysics. Simulation parameters are listed in Table S-1. Experimental SECM CVs are from Figure 3.

Effects of Potential Sweep Rate and Tip–Substrate Distance. We varied the sweep rate of the substrate potential and the tip–substrate distance to further validate the $EC_{ads}C_{mag}$ mechanism and reaction parameters determined by SECM-based CV. Specifically, the feedback branch of SECM-based CV was measured at potential sweep rates of v = 5, 10, 25, and 50 mV/s at a short tip–substrate distance of d = 2.1 μm in comparison with SECM-based CV in Figure 3 (v = 25 mV/s and d = 4.1 μm). All SECM-based CVs at the different potential sweep rates fitted well with theoretical CVs based on the $EC_{ads}C_{mag}$ mechanism (Figure S-5) to yield reaction parameters for each step (Table S-2). No magnetite formation was observed at 50 mV/s (i.e., $k_{m,f}$ was zero in Figure S-5A), where a sufficient amount of the Fe(II) intermediate was not formed during the faster potential cycle to deposit magnetite. Accordingly, the reverse peak of the feedback branch was lower at 50 mV/s than at 25 mV/s (Figure S-5B). The reverse peak was also suppressed as the potential sweep rate was reduced to 10 mV/s (Figure S-5C) and then to 5 mV/s (Figure S-5D). This result is attributed to slower adsorption and desorption of Fe(II)-TEA at a slower potential sweep rate (see k values in Table S-2).

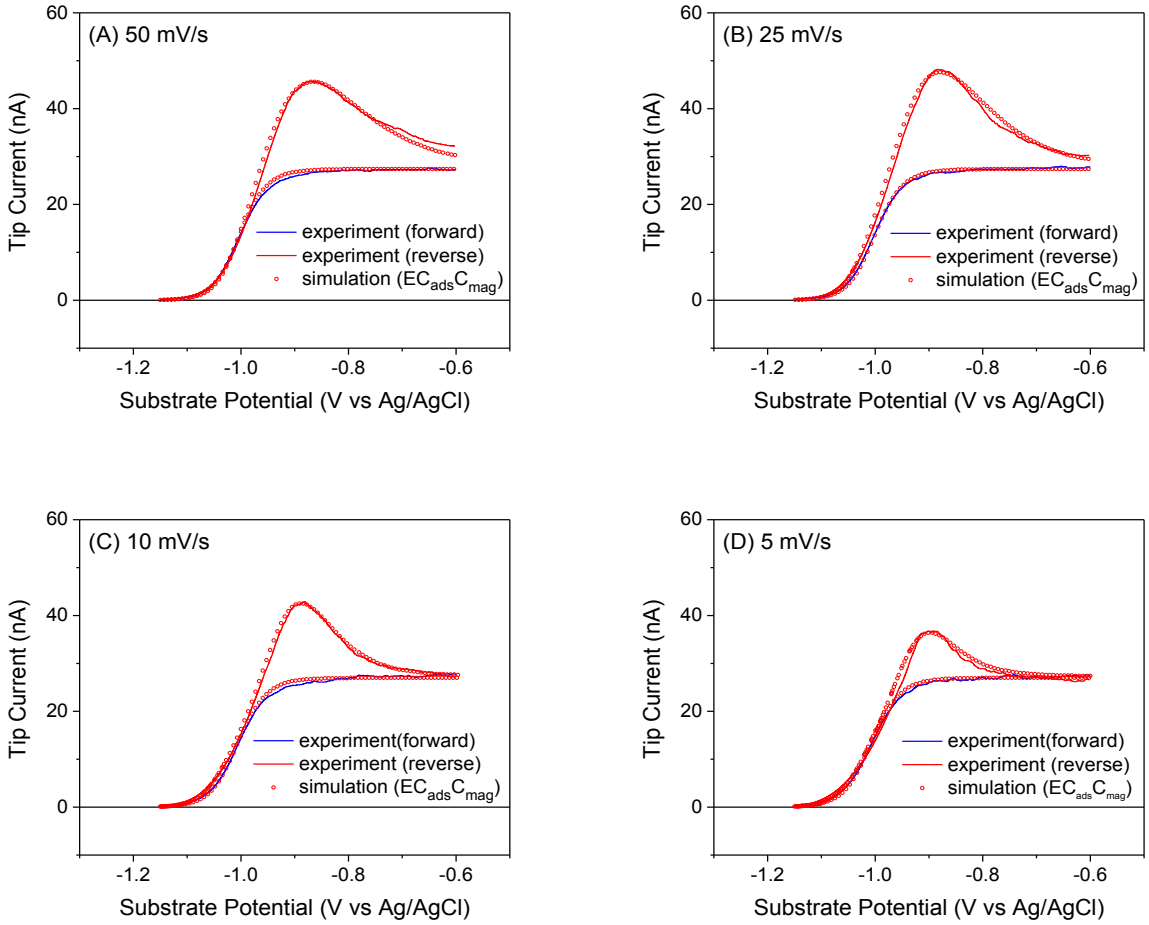

Figure S-5. Experimental SECM-based CVs at different potential sweep rates and theoretical CVs based on the $EC_{ads}C_{mag}$ mechanism. Experimental CVs were obtained with a 25 μm-diameter Au tip (E_T = –1.15 V vs Ag/AgCl) at a 2 mm-diameter Au substrate in a 5 M NaOH solution containing 5 mM Fe(III)–TEA. Simulation parameters are d = 2.1 μm and those listed in Table S-2.

Table S-2. Effects of Potential Sweep Rate on Parameters for Electrodeposition and Electrodissolution of Magnetite Based on the $EC_{ads}C_{mag}$ Mechanism.[a]

v (mV/s)	50	25	10	5
k^0 (cm/s)	0.13	0.13	0.13	0.13
$E^{0'}$ (V vs Ag/AgCl)	–1.022	–1.030	–1.024	–1.020
k (10^5 cm^3/s/mol)	2.0	2.0	0.51	0.26
$\beta_{Fe(II)}$ (10^5 cm^3/mol)	2.1	1.5	1.5	1.5
g'	1.9	2.7	2.7	2.7
$\Gamma^0_{Fe(II)}$ (10^{-9} mol/cm^2)	3.0	4.4	4.4	4.4
$k_{m,f}$ (10^{10} cm^6/s/mol^2)	0[b]	1.1	1.1	1.1
K_m (10^{10} cm^6/mol^2)	—[b]	1.9	1.1	1.0

[a] Figure S-5. [b] No magnetite was formed.

Double Potential Step Chronocoulometry. We determined the surface concentration of the Fe(II) intermediate adsorbed on the Au substrate by double potential step chronocoulometry[S-3] (Figure S-6A). In this measurement, the substrate current was monitored while the substrate potential was stepped from –0.6 V to –1.15 V for the formation of the adsorbed Fe(II) intermediate and then back to –0.6 V for the complete desorption of the intermediate (Figure 4B). No magnetite was formed either at –0.6 V or –1.15 V (Figure 4A). The duration of each step was 10 s. The resultant charge, $Q(t)$, was plotted for the forward step against the square root of time, $t^{1/2}$ (the top panel of Figure S-6B) to yield a good fit with

$$Q(t) = 2nFAc_0\sqrt{\frac{D_{\mathrm{Fe(III)}}t}{\pi}} + Q_{\mathrm{dl}} \qquad \text{(S-34)}$$

where A is the electrode area and Q_{dl} (= 1.15 μC) is the charge for double-layer charging. In this analysis, no adsorption of Fe(III)–TEA was assumed. On the other hand, the charge during the reverse step, $Q_{\mathrm{r}}(t)$, was defined by

$$Q_{\mathrm{r}}(t) = Q(t) - Q(\tau) \qquad \text{(S-35)}$$

where τ (= 10 s) is the switching time. $Q_{\mathrm{r}}(t)$ was plotted against θ as given by

$$\theta = \tau^{1/2} + (t-\tau)^{1/2} - t^{1/2} \qquad \text{(S-36)}$$

The $Q_{\mathrm{r}}(t)$ versus θ plot yielded a diffusion-controlled linear region (the bottom panel of Figure S-6B). The intercept, b, at $\theta = 0$ is given by[S-4]

$$b = nFA\Gamma(\tau) + Q_{\mathrm{dl}} \qquad \text{(S-37)}$$

where $\Gamma(\tau)$ is the surface concentration of redox-active species adsorbed on the substrate at the switching time. Eq S-37 with n = 1 yielded $\Gamma(\tau) = 5.4 \times 10^{-9}$ mol/cm^2 for the adsorbed Fe(II)

intermediate. This $\Gamma(\tau)$ value is affected by charging current, but close to $\Gamma^{0}_{\mathrm{Fe(II)}}$ values estimated by SECM-based CV, where the amperometric tip current does not involve charging current.

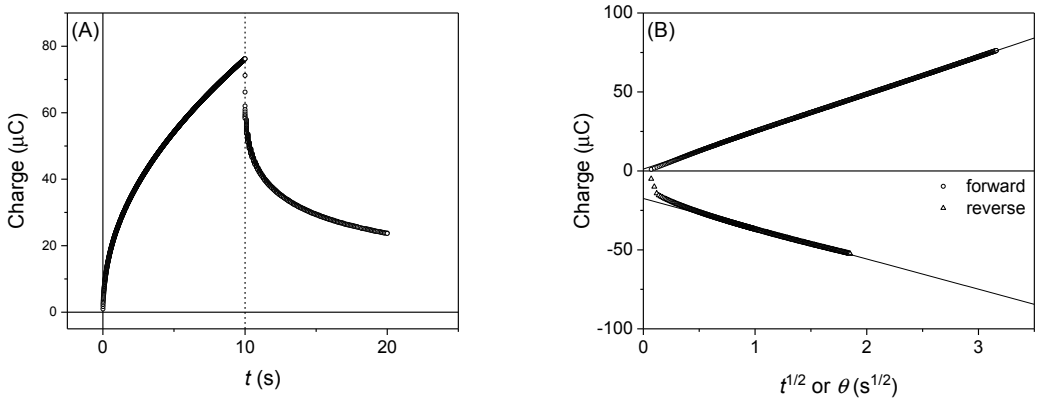

Figure S-6. (A) Double potential step chronocoulometry and (B) the corresponding Anson plots of 5 mM Fe(III)–TEA (1:2) at a 2 mm-diameter Au electrode in 5 M NaOH. Initial and final potentials, –0.6 V vs Ag/AgCl. Switching potential, –1.15 V vs Ag/AgCl.

EC Mechanism without Magnetite Formation. Here we compare experimental SECM-based CVs in Figure 3 with theoretical CVs based on the EC mechanism, where the chemical step was the adsorption of Fe(II)–TEA (eq 3) and was not coupled with the formation of magnetite (eq 4). This EC mechanism can be represented simply by setting $k_{m,f} = 0$ in the $EC_{ads}C_{mag}$ mechanism defined above. In Figures S-7A and S-7B, parameters were adjusted until the best fit was confirmed visually for both feedback and SG/TC branches. A good fit, however, was not obtainable for the reverse wave of the experimental feedback branch, which decayed more slowly than that of the simulated one. The experimental tip current was enhanced more than the simulated current beyond the peak potential (see the red arrow in Figure S-7A), where magnetite was dissolved to produce Fe(III)-TEA directly as well as indirectly by the oxidation of Fe(II)-TEA. The generation of Fe(III)-TEA from magnetite at these potentials was confirmed by the finite element simulation of the $EC_{ads}C_{mag}$ mechanism (Figure 4). Moreover, we employed the method of least squares in Figures S-7C and S-7D to ensure that the reverse peak of the experimental feedback branch can not be fitted well with the EC mechanism without magnetite formation (see the red arrow in Figure S-7C).

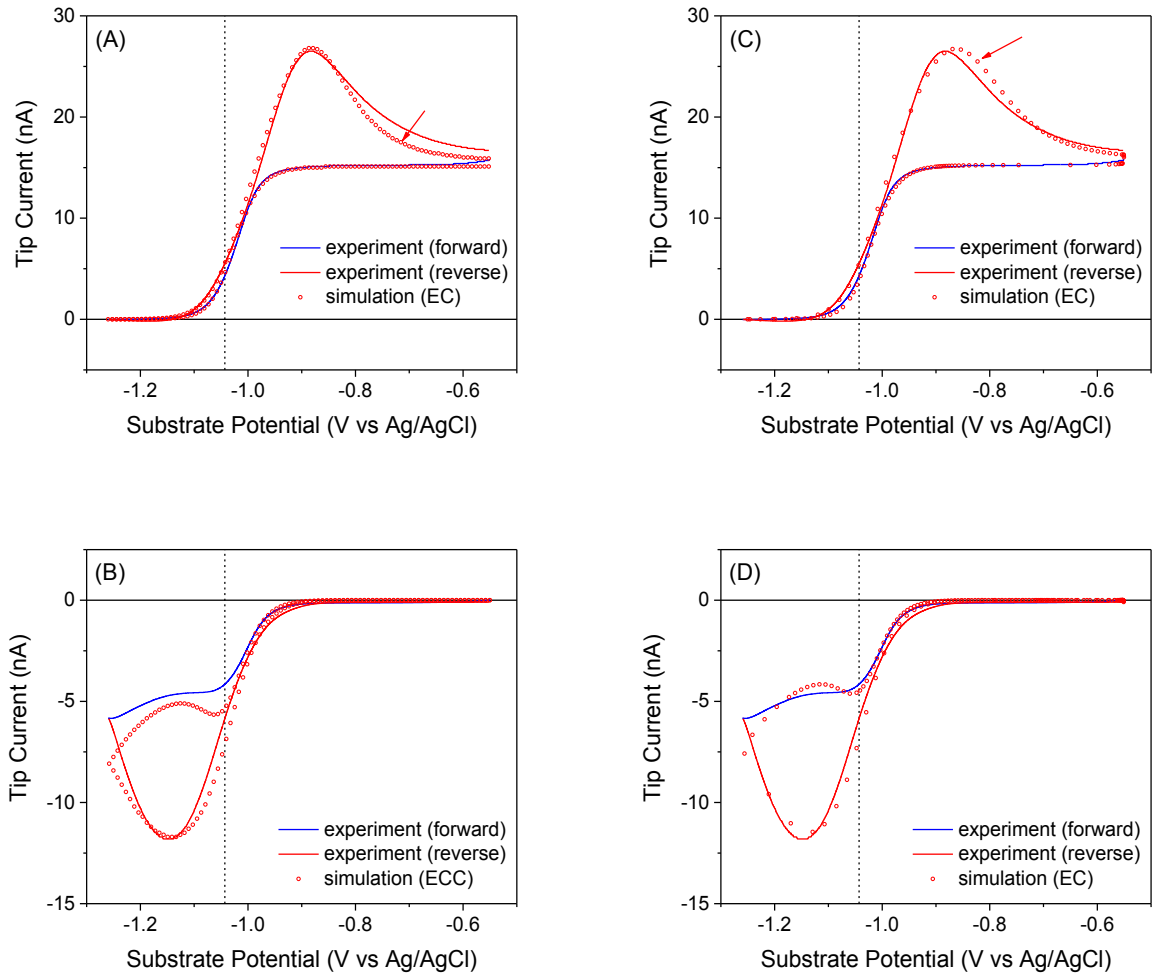

Figure S-7. Experimental SECM-based CVs from Figure 3 and CVs based on the EC mechanism without magnetite formation as fitted by (A) and (B) visual inspection and (C) and (D) the method of least squares. (A) and (C) are based on the feedback mode and (B) and (D) are based on the SG/TC mode. Simulation parameters are listed in Table S-3.

Table S-3. Reaction Parameters Determined from Both Feedback and SG/TC Branches for the EC Mechanism without Magnetite Formation.

Fitting method	Visual inspection[a]	Method of least squares[b]
k^0 (cm/s)	0.13	0.13
$E^{0\prime}$ (V vs. Ag/AgCl)	–1.038	–1.040
k (10^5 cm^3/s/mol)	1.2	1.3
$\beta_{Fe(II)}$ (10^5 cm^3/mol)	1.3	2.1
g'	3.5	3.1
$\Gamma^0_{Fe(II)}$ (10^{-9} mol/cm^2)	4.8	5.4

[a] Figures S-7A and S-7B. [b] Figures S-7C and S-7D.

EC Mechanism Based on One-Step Magnetite Formation. Experimental SECM-based CVs in Figure 3 were compared with theoretical CVs based on the EC mechanism with the one-step deposition of magnetite (eq 2). The corresponding model was obtained by modifying the aforementioned model of the $EC_{ads}C_{mag}$ mechanism as follows. In this EC mechanism, the adsorption of Fe(II)-TEA on the substrate surface was not considered (i.e., $k = 0$). The rate of magnetite formation, v_m, was given by

$$v_{\mathrm{m}} = k_{\mathrm{m,f}} \left\{ \left[c_{\mathrm{Fe(III)}} \right]^2 c_{\mathrm{Fe(II)}} - \frac{\Gamma_{\mathrm{Fe_3O_4}}}{K_{\mathrm{m}}} \right\} \tag{S-38}$$

Accordingly, the boundary condition for Fe(II)-TEA at the substrate surface was defined as

$$D_{\mathrm{Fe(II)}} \left[\frac{\partial c_{\mathrm{Fe(II)}}}{\partial z} \right]_{z=-d} = v_{\mathrm{et}} - v_{\mathrm{m}} \tag{S-39}$$

The dimensionless form of this boundary condition was given by

$$\gamma \left[\frac{\partial C_{\mathrm{Fe(II)}}}{\partial Z} \right]_{Z=-L} = V_{\mathrm{et}} - V_{\mathrm{m}} \tag{S-40}$$

where

$$V_{\mathrm{m}} = \kappa_{\mathrm{m,f}} \left\{ \left[C_{\mathrm{Fe(III)}} \right]^2 C_{\mathrm{Fe(II)}} - \frac{\theta_{\mathrm{Fe_3O_4}}}{\Lambda_{\mathrm{m}}} \right\} \tag{S-41}$$

with

$$\kappa_{\mathrm{m,f}} = \frac{k_{\mathrm{m,f}} a c_0^2}{D_{\mathrm{Fe(III)}}} \tag{S-42}$$

$$\Lambda_{\mathrm{m}} = \frac{c_0^2 K_{\mathrm{m}}}{a} \tag{S-43}$$

Figure S-8 compares experimental SECM-based CVs from Figure 3 with theoretical CVs based on the EC mechanism with one-step magnetite deposition. A good fit was not obtainable with this EC

mechanism, where magnetite was deposited and dissolved only around the formal potential. Subsequently, small peak-shaped responses based on the dissolution of magnetite were obtained during forward and reverse potential sweeps in SG/TC and feedback modes, respectively. The peak currents were maximized when both ET and chemical steps were diffusion-limited ($\lambda = \kappa_{m,f} = \kappa_{m,b} = 100$ in Figure S-8, where the normalized revers rete constant, $\kappa_{m,b}$, is equal to $\kappa_{m,f}/\Lambda_m$). Accordingly, each step of the EC mechanism was unresolvable to yield the overall reaction as

$$3\text{Fe(III)–TEA} + 8\text{OH}^- + \text{e}^- \rightleftharpoons \text{Fe}_3\text{O}_4 + 3\text{TEA} + 4\text{H}_2\text{O} \qquad \text{(S-39)}$$

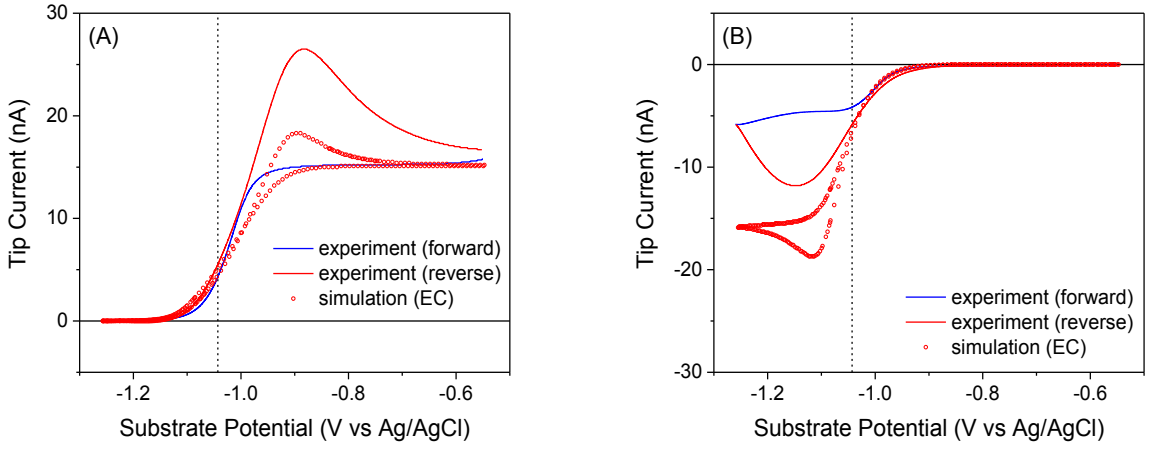

Figure S-8. Experimental SECM-based CVs from Figure 3 and theoretical CVs based on the EC mechanism with one-step magnetite formation. (A) and (B) are based on feedback and SG/TC modes, respectively. Simulation parameters are $k^0 = 0.16$ cm/s, $E^{0'} = -1.035$ V vs. Ag/AgCl, $k_{m,f} = 6.4 \times 10^9$ cm^7/s/mol^2, and $K_m = 5.0 \times 10^7$ cm^7/ mol^2.

Inhibitory Effect of the Adsorbed Fe(II) Intermediate on ET Kinetics. We employed the method of least squares to demonstrate that the reverse wave based on the SG/TC mode can not be fitted well (see the red arrow in Figure S-9B) when the inhibitory effect of the adsorbed Fe(II) intermediate on the ET kinetics of the Fe(III)-TEA/Fe(II)-TEA (eq 1) is not considered (i.e., $k^0_{app} = k^0$ in eq 10). This result confirms that the inhibitory effect is important during the reverse sweep when the surface coverage of the substrate with the adsorbed Fe(II) intermediate is high (Figure 4B).

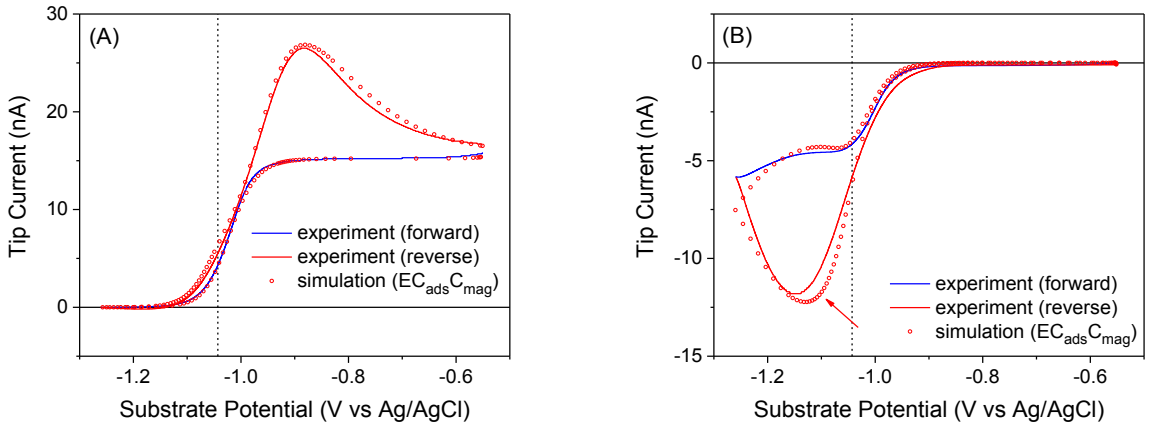

Figure S-9. Experimental and simulated SECM CVs in (A) feedback and (B) SG/TC modes when no inhibitory effect of the adsorbed Fe(II) intermediate on ET kinetics is considered. Simulated SECM CVs are based on the best fit to experimental SECM CVs in both modes by the method of least squares. Simulation parameters are $k^0 = 0.13$ cm/s, $E^{0'} = -1.046$ V vs. Ag/AgCl, $k = 2.1 \times 10^5$ cm^3/s/mol, $\beta_{Fe(II)} = 1.5 \times 10^5$ cm^3/mol, $g' = 3.3$, $\Gamma^0_{Fe(II)} = 5.5 \times 10^{-9}$ mol/cm^2, $k_{m,f} = 1.2 \times 10^{10}$ cm^6/s/mol^2, and $K_m = 2.2 \times 10^{10}$ cm^6/mol^2. Experimental SECM CVs are identical to those shown in Figure 3.

Fluxes Based on Chemical Steps at the Substrate Surface. We employed the finite element method to simulate normalized fluxes for chemical steps at the substrate surface (Figure 4) by using the parameters determined from SECM-based CVs (Table 1). A normalized flux is obtained by integrating the corresponding dimensionless rate over the substrate under the whole tip including Au and glass sheath. Specifically, the normalized flux based on the adsorption and desorption of Fe(II)–TEA, J_{ads}, is defined as

$$J_{ads} = \frac{2\pi \int_0^3 V_{ads} R dR}{9\pi} \tag{S-44}$$

where 9 is the normalized area whether the flux is integrated.

The normalized flux based on the deposition and dissolution of magnetite, J_m, is given by

$$J_m = \frac{2\left(2\pi \int_0^3 V_m R dR \right)}{9\pi} \tag{S-45}$$

where a factor of 2 is multiplied because the deposition and dissolution of magnetite consumes and produces 2 molecules of Fe(III)–TEA, respectively (see eq 4).

Effects of Switching Potential. SECM-based CVs at various switching potentials were analyzed by employing the finite element simulation (Figure S-10). Parameters that are dependent on switching potentials are listed in Table S-4. Other parameters are identical to those listed in Table 1.

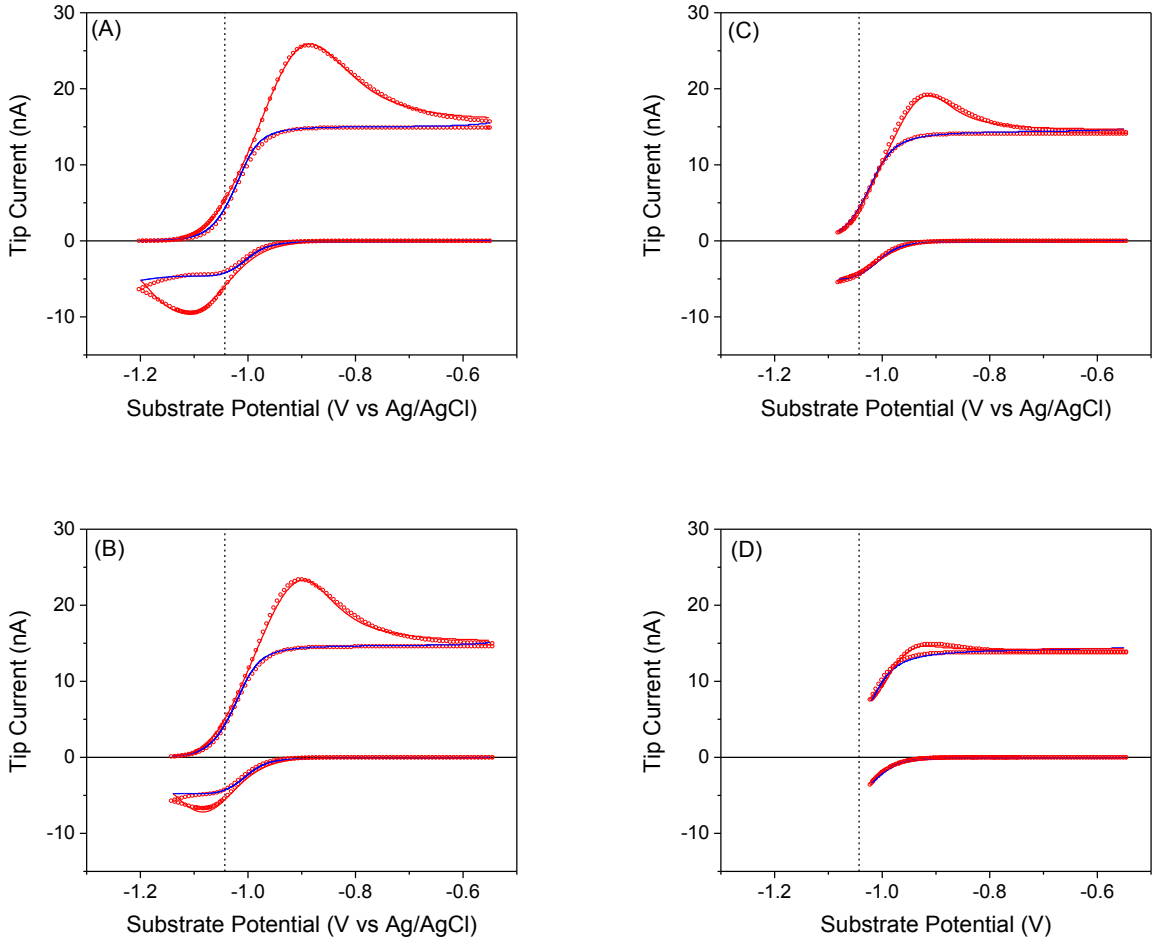

Figure S-10. SECM-based CVs in feedback (red) and SG/TC (blue) modes with a 25 μm-diameter Au tip at a 2 mm-diameter Au substrate in a 5 M NaOH solution containing 5 mM Fe(III)–TEA. E_T = –1.12 and –0.75 V vs Ag/AgCl for the respective operation modes. Switching potentials are (A) –1.20, (B) –1.14, (C) –1.08, and (D) –1.02 V vs Ag/AgCl. Potential sweep rate, 25 mV/s. Blue and red lines represent the forward and reverse branches of experimental CVs, respectively, whereas simulated CVs are shown by circles.

Table S-4. Effects of Switching Potential on Parameters for Electrodeposition and Electrodissolution of Magnetite Based on the $EC_{ads}C_{mag}$ Mechanism.[a]

Switching Potential (V[b])	–1.23[c]	–1.20[d]	–1.17[c]	–1.14[d]	–1.11[c]	–1.08[d]	–1.05[c]	–1.02[d]
$\Gamma^{0}_{Fe(II)}$ (10^{-9} mol/cm^2)	5.3	5.0	4.6	4.4	3.9	3.8	3.4	2.8
$\beta_{Fe(II)}$ (10^5 cm^3/mol)	1.7	1.7	1.8	1.8	2.1	2.1	2.1	2.1
g'	3.2	3.0	2.8	2.7	2.4	2.3	2.1	1.7
K_m (10^{10} cm^6/mol^2)	1.7	1.6	1.2	0.96	0.60	0.36	0.12	—[e]

[a] Other parameters are listed in Table 1. [b] Against Ag/AgCl. [c] Figure 6. [d] Figure S-10. [e] No magnetite formation.

REFERENCES

(S-1) Cornut, R.; Lefrou, C. *J. Electroanal. Chem.* **2007**, *608*, 59.

(S-2) Nioradze, N.; Kim, J.; Amemiya, S. *Anal. Chem.* **2011**, *83*, 828.

(S-3) Anson, F. C. *Anal. Chem.* **1966**, *38*, 54.

(S-4) Puy, J.; Pla, M.; Mas, F.; Sanz, F. *J. Electroanal. Chem.* **1988**, *241*, 89.